FUDMA Journal of Sciences (FJS)
ISSN online: 2616-1370
ISSN print: 2645 - 2944
Vol. 10 No. 24, December, 2026, pp 177 – 186
DOI: https://doi.org/10.33003/fjs-2026-1024-6374

Synthesis, Characterization and Fixed-Bed Fluoride Adsorption Performance of a Banana Pseudostem Cellulose–Montmorillonite Composite

Wilson Lamayi Danbature, *Ibrahim Abubakar Sani, Zaccheus Shehu, Usman Adamu Abubakar, and Imrana Muhammad Abdullahi

Department of Chemical Sciences, Gombe State University, Gombe State, Nigeria.

*Corresponding authors' email: abubakaribrahimsani37@gmail.com

Received: 20 Oct. 2026
Accepted: 10 Nov. 2026
Published: 12 Nov. 2026

ABSTRACT
Excessive fluoride in drinking water poses significant public-health concerns, particularly in communities that depend on untreated groundwater. This study synthesized a banana pseudostem cellulose–montmorillonite composite and evaluated its performance for fluoride removal in a continuous fixed-bed adsorption column. Cellulose was extracted from banana pseudostem and combined with montmorillonite by aqueous blending with citric-acid-assisted preparation. The composite was characterized by scanning electron microscopy, energy-dispersive X-ray spectroscopy, X-ray diffraction, Fourier-transform infrared spectroscopy and Brunauer–Emmett–Teller surface-area analysis. The reported specific surface area increased from 2.0 m^2/g for untreated cellulose to 16.5 m^2/g for the composite. Fixed-bed experiments examined the effects of adsorbent mass, contact time, flow rate and influent fluoride concentration. The maximum reported removal efficiency was 79.83% at an adsorbent mass of 10 g. Removal efficiency decreased from 76.36% to 55.42% over five reuse cycles. Treatment of borehole water from five communities in Gombe State gave removal efficiencies of 61.69% to 76.36%. Reported column-model coefficients could not be independently validated because the raw breakthrough data and model-specific conditions were unavailable. The findings suggest that the composite has potential for fluoride adsorption. However, mass-balance analysis, experimental replication, leaching assessment and verification of treated-water quality are necessary before practical application.

Keywords: Adsorption, Banana Pseudostem, Fixed-Bed Column, Fluoride, Montmorillonite, Cellulose, Water Treatment

INTRODUCTION

Fluoride is naturally released into groundwater through the weathering and dissolution of fluoride-bearing minerals, and its concentration is influenced by geology, pH, alkalinity, residence time and evaporation (Solanki *et al*., 2022; World Health Organization [WHO], 2022). Low concentrations can contribute to dental-caries prevention, but prolonged exposure above recommended limits increases the risk of dental fluorosis, skeletal fluorosis and other systemic effects (Solanki *et al*., 2022; WHO, 2022). The WHO guideline value for fluoride in drinking water remains 1.5 mg/L, with the caution that national limits may need to be lower where water consumption, climate or dietary fluoride exposure is high (WHO, 2022). Fluoride contamination is especially important in regions where groundwater is the main drinking-water source and centralized treatment is limited (Solanki *et al*., 2022; Wan *et al*., 2021). In north-eastern Nigeria, a groundwater-quality investigation around Bogoro, Bauchi State, likewise found fluoride, together with turbidity and iron, among the parameters above the permissible limits applied in that study (Yohanna *et al*., 2022).

Conventional defluoridation techniques include precipitation-coagulation, ion exchange, reverse osmosis, nanofiltration, electrodialysis and adsorption (Solanki *et al*., 2022; Wan *et al*., 2021). Membrane systems can achieve high rejection, but cost, energy demand, concentrate management and fouling reduce suitability in low-resource settings (Wan *et al*., 2021). Coagulation and ion-exchange methods can remove fluoride, but they require chemical supply, regeneration or sludge management that can limit field adoption (Wan *et al*., 2021; Kumari *et al*., 2021). Adsorption remains attractive because it can operate with simple equipment, can use low-cost adsorbents and can be configured for continuous columns (Kumari *et al*., 2021; Wan *et al*., 2021).

Montmorillonite is a layered smectite clay with swelling interlayers, exchangeable cations and active edge sites that make it useful for pollutant adsorption (Zango *et al*., 2022). Raw montmorillonite may aggregate, release fines and show limited anion affinity in continuous systems, so surface modification and composite formation are commonly used to improve stability and accessibility (Zango *et al*., 2022; Zhang, 2024). Recent modified montmorillonite systems have shown improved fluoride uptake through electrostatic attraction, ligand exchange, ion exchange and surface-complexation pathways (Nehra *et al*., 2022; Zhang, 2024). These properties make montmorillonite a suitable mineral phase for developing low-cost fluoride adsorbents (Zango *et al*., 2022; Zhang, 2024). In the present composite, montmorillonite is expected to supply the principal fluoride-binding sites (edge Al–OH and Si–OH groups and exchangeable cations), whereas cellulose is expected to act mainly as a support that limits clay dispersion and fines loss in a packed bed.

Cellulose is renewable, biodegradable and rich in hydroxyl groups, which makes it useful as a support matrix for water-treatment materials (Das *et al*., 2022; Nascimento *et al*., 2023). Banana pseudostem is an agricultural residue that contains recoverable cellulose and can be converted into value-added materials instead of being discarded (Merais *et al*., 2022; Nascimento *et al*., 2023). Alkaline treatment and bleaching remove lignin, hemicellulose and extractives while

exposing cellulose surfaces that can interact with inorganic phases (Merais *et al*., 2022; Nascimento *et al*., 2023). Nanocellulose and cellulose-based composites are promising for water purification because their surface chemistry can support adsorption, immobilization of mineral phases and formation of porous networks (Das *et al*., 2022).

Combining cellulose with montmorillonite can reduce clay aggregation, improve bed handling and provide a hybrid surface containing both polymer hydroxyl groups and aluminosilicate sites (Das *et al*., 2022; Zango *et al*., 2022). Earlier cellulose–clay and biopolymer–clay fluoride adsorbents include magnetite–montmorillonite-encapsulated cellulose beads (Nehra *et al*., 2022) and bentonite–chitosan materials cross-linked with a dicarboxylic acid and decorated with metal ions (Nagaraj *et al*., 2020). These materials show the value of immobilizing clay within a biopolymer framework for adsorption and reusability, but they rely on additional magnetic, metal-ion or chitosan components that add preparation complexity and cost. The use of locally available banana pseudostem cellulose with locally sourced montmorillonite could reduce material cost and support circular use of agricultural waste (Das *et al*., 2022; Nascimento *et al*., 2023). Evidence on simple banana-cellulose–montmorillonite adsorbents under continuous flow is still limited, which creates a research gap for fixed-bed fluoride-removal studies (Kumari *et al*., 2021; Wan *et al*., 2021).

Citric acid was included to promote association between cellulose and the mineral phase. Hydrogen bonding is plausible, but the preparation temperatures and the available characterization do not establish covalent ester cross-linking. The role of citric acid was not tested against an otherwise identical preparation without citric acid.

Fixed-bed columns better approximate continuous water treatment than batch tests because they reveal breakthrough, exhaustion, bed utilization and hydraulic behavior (Kumari et al., 2021; Mani & Bhandari, 2022). Column performance is affected by adsorbent mass, bed depth, flow rate, influent concentration, particle size and mass-transfer resistance (Kumari et al., 2021; Mani & Bhandari, 2022). Thomas and Yoon-Nelson model applications are useful for interpreting breakthrough behavior and comparing service performance in fluoride-removal columns (Kumari et al., 2021; Mani & Bhandari, 2022).

Existing fixed-bed defluoridation systems include acid-modified alumina for industrial wastewater (Kumari *et al*., 2021), metal-complexed polyvinyl alcohol hydrogel beads (Mani & Bhandari, 2022) and acid-treated bentonite optimized on fluoride solutions (Kalsido *et al*., 2021). These systems depend on metal-based, synthetic-polymer or chemically activated media, and they leave open the performance of a simple agricultural-waste cellulose–montmorillonite medium in continuous flow. The present study addresses this by using a low-temperature aqueous preparation from banana pseudostem cellulose and locally sourced montmorillonite, and by evaluating the composite not only with synthetic feed solutions but also with borehole water from five communities, over five reuse cycles and with Thomas and Yoon–Nelson column models.

This study aimed to synthesize and characterize a banana pseudostem cellulose–montmorillonite composite and evaluate its fluoride removal performance, operational characteristics and reusability in a continuous fixed-bed adsorption system.

MATERIALS AND METHODS

Materials and Reagents

The chemicals and reagents used in the study were montmorillonite clay, banana pseudostem cellulose, hydrochloric acid, sodium hydroxide, hydrogen peroxide, acetic acid, citric acid, sodium fluoride for fluoride standards and synthetic fluoride feed preparation, and distilled water. All reagents were of analytical grade where available, and all glassware and sample containers were cleaned before use. Residual fluoride was determined by a calibrated UV-visible colorimetric method (Section 2.6.6).

The principal equipment and instruments included an analytical balance, glass beakers, measuring cylinders, volumetric flasks, magnetic stirrer or hot-plate stirrer, drying oven, grinder or mortar and pestle, pH meter, polyethylene terephthalate sample bottles, glass fixed-bed column, glass wool support, peristaltic pump, UV-visible spectrophotometer, SEM-EDX instrument, XRD instrument, FTIR spectrometer and BET surface-area analyzer.

Purification and Acid Activation of Montmorillonite

Raw montmorillonite clay was dispersed in distilled water, agitated and allowed to settle so that coarse mineral impurities could be separated by decantation. The purified fraction was oven-dried at 105 °C for 24 h. Where acid activation was applied, the dried clay was contacted with 1 M HCl at 80 °C for 4 h under continuous stirring, washed repeatedly with distilled water until approximately neutral pH was obtained, and dried again at 105 °C. The activation step was intended to remove soluble impurities, improve pore accessibility and increase the availability of surface and edge sites while retaining the clay framework.

Extraction of Cellulose from Banana Pseudostem

Banana pseudostems were washed, chopped and dried at 80 °C. The dried biomass was treated with 5% NaOH at 90 °C for 4 h to remove lignin, hemicellulose, extractives and part of the noncellulosic matrix. After repeated washing to near-neutral pH, the material was bleached with a 1:1 hydrogen peroxide–acetic acid mixture at 70 °C for 2 h. The resulting product was washed and dried and is referred to throughout this manuscript as banana pseudostem cellulose. The preparation did not include acid hydrolysis to produce cellulose nanocrystals or high-shear fibrillation to produce cellulose nanofibrils, and no particle dimension was measured directly by TEM, AFM or DLS; the product is therefore not described as nanocellulose. This extraction sequence is consistent with alkaline delignification and oxidative bleaching routes used to recover cellulose from banana pseudostem (Merais *et al*., 2022; Nascimento *et al*., 2023).

Formation of the Cellulose–Montmorillonite Composite

Twenty grams of prepared montmorillonite was dispersed in 200 mL of distilled water and stirred for 30 min to obtain a uniform slurry. Ten grams of extracted banana pseudostem cellulose was added slowly to the montmorillonite slurry while stirring to ensure even mixing, giving a clay-to-cellulose mass ratio of 2:1. Five millilitres of 1 M citric acid was added to promote association between the cellulose and montmorillonite phases. The mixture was heated at 70 °C and stirred continuously for 4 h, then oven-dried at 80 °C for 12 h to remove excess moisture. The dried cellulose–montmorillonite composite was ground into a fine powder and stored in an airtight container before characterization and fixed-bed column packing. The term composite is used here for the hybrid material in which montmorillonite is dispersed

within, and bound to, the cellulose matrix. No claim is made that the product is a nanocomposite, because particle size below 100 nm was not demonstrated directly.

Characterization

Scanning Electron Microscopy

Scanning electron microscopy (SEM) was used to compare the surface morphology of the extracted banana pseudostem cellulose and the prepared cellulose-montmorillonite composite. The samples were mounted on suitable stubs and examined at the reported electron high tension of 15 kV using secondary-electron or variable-pressure secondary-electron imaging at different magnifications. The micrographs were assessed for fibre organization, particle aggregation, surface roughness, visible pores and the distribution of mineral domains.

Energy-Dispersive X-Ray Spectroscopy

Energy-dispersive X-ray spectroscopy (EDX), coupled to the SEM, was used for semiquantitative identification of elements in representative fields of the cellulose and composite. Elemental peaks and atomic percentages were obtained from the instrument output. Because EDX is field-specific and semiquantitative, the reported values describe the analyzed areas and were used to compare the organic cellulose-rich material with the aluminosilicate-rich composite.

XRD, FTIR and BET Analyses

X-ray diffraction (XRD) was used to evaluate crystalline features. Crystallite size was reported from peak broadening using the Scherrer relation, D = K lambda/(beta cos theta), where D is the apparent crystallite size, K is the shape factor, lambda is the X-ray wavelength, beta is the full width at half maximum in radians, and theta is the Bragg angle. Fourier transform infrared (FTIR) spectroscopy was used to identify the main hydroxyl, aliphatic, carbohydrate and clay-related vibrational bands. Brunauer-Emmett-Teller (BET) nitrogen adsorption analysis was used to estimate specific surface area and pore characteristics.

Fixed-Bed Column Adsorption Experiment

Column Set-Up

Continuous adsorption was carried out at room temperature in five vertical glass columns, each with an internal diameter of 2.5 cm and an overall height of 40 cm, packed with 3, 6, 8, 10 and 12 g of the cellulose–montmorillonite composite, respectively. A layer of glass wool was placed at the bottom of the column to support the packed composite, improve flow distribution and prevent loss of adsorbent particles. Fluoride-containing water was delivered through the packed bed with a peristaltic pump at a controlled flow rate. Effluent fractions were collected at specified operating times and the run was continued for the selected experimental period. This arrangement followed the operating principles used in published continuous packed-bed studies (Nwabanne & Igbokwe, 2012; Yahya *et al*., 2020).

Packed Adsorbent Mass and Bed Condition

The effect of the packed bed was investigated using 3, 6, 8, 10 and 12 g of dry composite. These values are expressed as packed adsorbent mass (g) rather than bed height (cm). For each run, the selected mass was placed above the glass-wool support and the other operating conditions were kept unchanged within that experimental series. Varying the amount of packed adsorbent while holding the influent condition and flow constant is consistent with established fixed-bed procedures for evaluating the number of available adsorption sites and the length of the active mass-transfer zone (Yahya *et al*., 2020).

Contact Time

The effect of contact (operating) time was evaluated at elapsed column operating times of 5, 15, 30, 45 and 60 min. A 10 g packed mass and an influent fluoride concentration of 12.5 mg/L were maintained for this series. Effluent was collected at each stated time and analyzed for residual fluoride. In a continuous column, these values represent sampling or operating time rather than a directly measured empty-bed contact time. The results were used to identify the operating period at which the highest removal occurred.

Influent Flow Rate

Flow rate was varied at 5, 10, 15, 20 and 25 mL/min using the peristaltic pump. The packed adsorbent mass, influent concentration and operating time were held at 10 g, 12.5 mg/L and 45 min, respectively. A separate fresh or regenerated bed was operated at each selected flow rate, and the effluent was collected for residual-fluoride measurement. This one-variable-at-a-time arrangement is commonly used to examine the balance between residence time, external mass transfer and bed saturation in fixed-bed systems (Nwabanne & Igbokwe, 2012; Yahya et al., 2020).

Initial Fluoride Concentration

The effect of influent fluoride concentration was studied using synthetic feed solutions of 2.5, 5.0, 7.5, 10.0 and 12.5 mg/L prepared from sodium fluoride. The column contained 10 g of the composite and was operated for 45 min at 5 mL/min for this series. Only the influent concentration was changed, which allowed its effect on the concentration driving force and bed utilization to be assessed (Yahya et al., 2020).

Determination of Residual Fluoride and Column Uptake

Residual fluoride in each influent and effluent sample was measured using a calibrated UV-visible colorimetric procedure. Sodium-fluoride standards were analyzed, absorbance was read with the UV-visible spectrophotometer, and the calibration relationship was used to convert sample absorbance to fluoride concentration. The analytical procedure followed standard water-analysis guidance (American Public Health Association *et al*., 2023).

$$\text{Removal (\%)} = [(C_0 - C_t) / C_0] \times 100 \quad (1)$$

Where C0 is the influent fluoride concentration (mg/L) and Ct is the effluent concentration (mg/L) at operating time t.

$$q_{total} = (Q / 1000) \int \text{ from 0 to } t_{total} (C_0 - C_t)\, dt \quad (2)$$

$$q_e = q_{total} / m \quad (3)$$

Where qtotal is the total mass of fluoride retained by the bed (mg), Q is the volumetric flow rate (mL/min), ttotal is the total column operating time (min), qe is the column adsorption capacity (mg/g), and m is the dry adsorbent mass (g). Equation (2) requires integration of the measured influent–effluent concentration difference over time. The available summary observations do not permit independent evaluation of that integral; no independently validated integrated capacity is therefore reported here.

Column Adsorption Models

Thomas Model

The Thomas model was applied to estimate the apparent column adsorption capacity and the Thomas rate constant. It assumes Langmuir-type adsorption-desorption behaviour, plug flow through the bed and negligible axial dispersion,

with the overall rate represented by second-order reversible reaction kinetics. The nonlinear and linear forms used for the fixed-bed data were (Nwabanne & Igbokwe, 2012):

$C_t / C_o = 1 / \{1 + \exp[(kTh\ q_om / Q) - kTh\ C_ot]\}$ (4)

$\ln[(C_o / C_t) - 1] = (kTh\ q_om / Q) - kTh\ C_ot$ (5)

where C0 and Ct are the influent and effluent fluoride concentrations (mg/L), respectively, kTh is the Thomas rate constant, q0 is the apparent maximum adsorption capacity of the adsorbent (mg/g), m is the adsorbent mass (g), Q is the volumetric flow rate, and t is the operating time (min). The slope and intercept of the plot of ln[(C0/Ct) - 1] against t were used to obtain the model parameters. The Thomas rate constant is expressed in L mg^{-1} min^{-1}, with Q converted to L min^{-1} when Equations (4) and (5) are evaluated.

Yoon-Nelson Model

The Yoon-Nelson model was used to describe the probability of adsorbate breakthrough and to estimate the time required for 50% breakthrough. The model does not require detailed information about the adsorbent properties or the adsorbate mechanism. Its nonlinear and linear forms were (Nwabanne & Igbokwe, 2012; Yahya et al., 2020):

$C_t / C_o = 1 / \{1 + \exp[kYN(\tau - t)]\}$ (6)

$\ln[C_t / (C_o - C_t)] = kYNt - kYN\tau$ (7)

Where kYN is the Yoon-Nelson rate constant (min^{-1}), tau is the time required for 50% breakthrough (min), t is the column operating time (min), C0 is the influent concentration and Ct is the effluent concentration. A plot of ln[Ct/(C0 - Ct)] against t gives a slope of kYN and an intercept of -kYN tau.

Linear least-squares regression was reported for Equations (5) and (7). The underlying time–concentration records and complete fitting conditions were not available for independent refitting. The two linearized response variables are exact negatives of each other. Consequently, fitting both to the same observations with an intercept must give equal R^2 values and opposite regression coefficients. The differing R^2 values reported in the summary require verification; neither model can be ranked above the other on this basis.

Regeneration and Reusability

After each adsorption run used for the reusability study, the fluoride-loaded composite was regenerated in the column by passing 0.1 M sodium hydroxide through the exhausted bed at 5 mL/min for 30 min to desorb retained fluoride. The bed was then rinsed with distilled water at the same flow rate until the effluent reached approximately neutral pH. The regenerated material was reused under constant adsorption conditions of 10 g packed mass, 12.5 mg/L influent fluoride, 5 mL/min flow rate and 45 min operating time. The adsorption–regeneration sequence was repeated for five cycles. Sodium hydroxide is a commonly used fluoride desorbent in fixed-bed regeneration, while maintaining constant operating conditions across cycles permits direct comparison of retained performance (Kumari *et al*., 2021).

Borehole-Water Sample Collection and Analysis

Borehole-water samples were collected from Herwagana in Gombe LGA, Bare in Billiri LGA, Kalering in Kaltungo LGA, Liji in Yamaltu Deba LGA and Anguwan Baraya in Tumu, Akko LGA, Gombe State. Pre-cleaned polyethylene terephthalate bottles were rinsed with the source water before filling, labelled with the location and sampling information, closed without unnecessary headspace and transported in a clean cooler to the laboratory. Sampling containers, handling and preservation followed standard procedures for drinking-water examination (American Public Health Association et al., 2023).

Field measurements comprised pH, electrical conductivity, total dissolved solids, turbidity and dissolved oxygen, using calibrated portable meters or field instruments appropriate to each parameter. Instrument probes were rinsed between samples and readings were recorded after stabilization. In the laboratory, total hardness was determined by EDTA complexometric titration and chloride by argentometric titration. Fluoride was measured by the same calibrated UV-visible colorimetric procedure used for the synthetic solutions. The borehole waters were then treated in the fixed-bed column using 10 g of composite, a flow rate of 15 mL/min and an operating time of 45 min. Influent and effluent fluoride concentrations were used to calculate removal by Equation (1). The field and laboratory analyses followed standard water-analysis procedures (American Public Health Association et al., 2023).

Replication and Statistical Analysis

Replicate-level records, analytical duplicates and uncertainty estimates were not available for this revision. The summarized observations are therefore presented descriptively, without error bars, significance tests or claims of statistically significant differences. The absence of accessible replicate records does not establish that no replicate measurements were performed.

RESULTS AND DISCUSSION

Morphology and Elemental Composition

Surface Morphology

The banana-derived material shown in Figure 1A is cellulose. Its micrograph showed a compact, heterogeneous fibrous surface with rounded and partially fused domains. The cellulose-montmorillonite composite in Figure 1B showed a more irregular granular texture, dispersed mineral-rich regions and visible interparticle voids. The difference arises because cellulose is the isolated organic biopolymer matrix, while the composite contains that cellulose combined with the layered montmorillonite mineral phase. The rougher, heterogeneous surface supports successful incorporation of the clay and may provide more accessible transport paths and external adsorption sites, although hydraulic behaviour also depends on particle-size distribution, packing density and swelling.

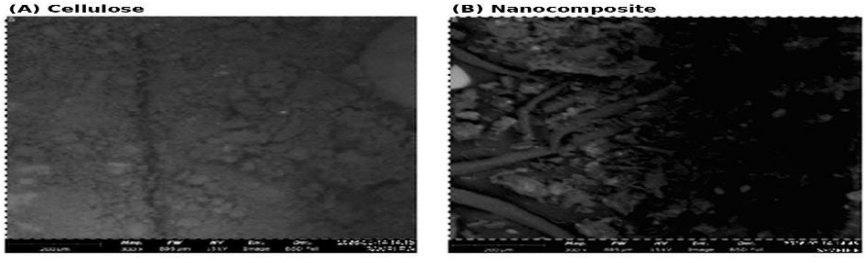


Figure 1: Scanning electron micrographs of (A) banana pseudostem cellulose and (B) the synthesized cellulose-montmorillonite composite

Elemental Composition

EDX quantified nine elements in the banana pseudostem cellulose and nine elements in the cellulose-montmorillonite composite (Figure 2). The cellulose contained C 48.13%, O 27.95%, Fe 9.69%, Mn 3.38%, Cu 3.36%, Ti 2.61%, K 2.46%, Zn 1.49% and S 0.94% by atomic concentration. Carbon and oxygen were dominant, as expected for a carbohydrate-rich cellulose material, while the lower-level elements may reflect residual minerals in the biomass, processing water, sample preparation or the specific field analyzed. The composite contained Si 71.39%, Al 12.05%, P 7.71%, Ca 2.73%, Zn 2.01%, Na 1.47%, Fe 1.18%, S 0.75% and C 0.72%. The shift from carbon-oxygen dominance in the cellulose to silicon-aluminium dominance in the composite is consistent with a silicon- and aluminium-rich mineral region. The listed composite elements sum to approximately 100%, but oxygen is absent from the reported list despite its expected presence in an aluminosilicate. The elemental selection and normalization basis require verification. EDX is semiquantitative and field-specific, so these percentages should be interpreted as the composition of the analyzed regions rather than the bulk material.

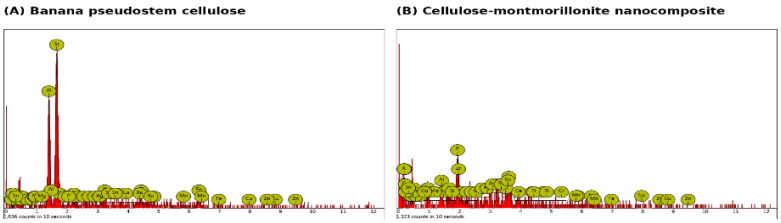


Figure 2: Energy-dispersive X-ray spectra of (A) banana pseudostem cellulose and (B) the cellulose-montmorillonite composite

X-ray Diffraction

The cellulose diffractogram contained prominent reflections near 32.28° and 46.24° 2θ superimposed on a broad background, and Scherrer analysis gave an apparent crystallite size of 45.52 nm. The composite pattern displayed a broad maximum centered in the lower-angle region and a reported prominent reflection near 16.17° 2θ, with an apparent crystallite size of 49.38 nm (Figure 3). The broad scattering is compatible with a material containing both disordered cellulose and a layered clay phase. The increase in apparent crystallite size should not be interpreted as direct proof of larger whole particles because Scherrer analysis measures coherent diffracting domains and is sensitive to strain, instrumental broadening, and peak selection.

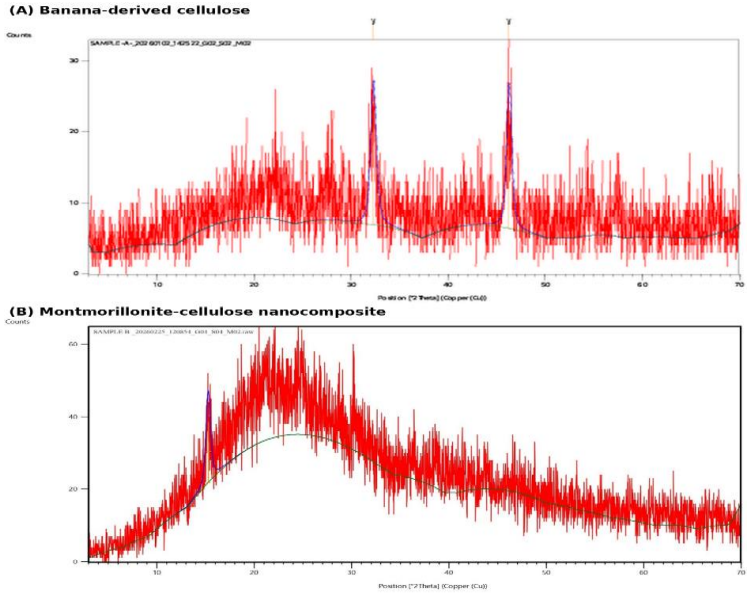


Figure 3: X-ray diffraction patterns of (A) banana pseudostem cellulose and (B) the cellulose-montmorillonite composite. The reported apparent crystallite sizes were 45.52 and 49.38 nm, respectively

A separate raw-clay diffractogram, full peak table, instrumental broadening correction and peak-indexing records were not available. The reported reflections near 32.28° and 46.24° should not be assigned to cellulose without phase identification, since residual crystalline salts or other mineral phases could contribute. The available summary does not establish montmorillonite intercalation, basal spacing or phase purity. Scherrer sizes are provisional coherent-domain estimates and do not demonstrate nanoscale particle dimensions.

FTIR Functional-Group Analysis

The cellulose and composite FTIR spectra (Table 1) shared a broad band near 3402 cm^{-1}, assigned to hydrogen-bonded O-H stretching, and aliphatic C-H stretching bands near 2924 and 2854-2855 cm^{-1}. A band near 1634-1640 cm^{-1} may include absorbed-water bending and contributions from residual unsaturated or carbonyl-containing components. Carbohydrate-related C-O and C-O-C vibrations occur in the fingerprint region near 1036-1155 cm^{-1}. The composite retained these cellulose-associated features but also showed

additional low-wavenumber mineral vibrations near 885, 671, and 615 cm^{-1}. The coexistence of hydroxyl-rich organic bands and mineral-region bands supports incorporation of montmorillonite into the cellulose matrix.

Table 1: Principal FTIR Bands Reported for the Cellulose and Composite

Band Region (cm^{-1})	Cellulose	Composite	Probable Assignment
3402–3240	3402, 3248	3402, 3240	Hydrogen-bonded O-H stretching in cellulose, surface hydroxyls, and adsorbed water
2924–2854	2924, 2855	2924, 2854	Aliphatic C-H stretching of cellulose and residual organic groups
1640–1634	1640	1634	H-O-H bending of adsorbed water, with possible contribution from residual unsaturated groups
1410–1320	1408, 1321	1410, 1320	CH2 bending, O-H deformation, and cellulose skeletal vibrations
1155–1036	1036	1155, 1037	C-O-C and C-O stretching of polysaccharides, with clay Si-O contribution near the lower fingerprint region
885–521	857, 794, 521	885, 671, 615	Beta-glycosidic and mineral lattice vibrations, including Si-O and Al-O related modes

The broad O-H region is relevant to adsorption because hydroxylated surfaces can interact with hydrated fluoride through hydrogen bonding and can participate indirectly in ion exchange or ligand-exchange reactions when associated with protonated edge sites or mineral cations. FTIR alone cannot prove a specific fluoride-binding mechanism. Such a claim would require spectra before and after adsorption, pH-dependent surface charge data, and ideally X-ray photoelectron spectroscopy or solid-state nuclear magnetic resonance. The present FTIR result therefore supports composite formation and the presence of potentially reactive hydroxyl and aluminosilicate groups, rather than identifying a single dominant adsorption pathway.

Surface Area and Pore Characteristics

The untreated cellulose had a reported BET surface area of 2.0 m^2/g and a reported pore size of 3 nm. Composite formation increased the surface area to 16.5 m^2/g and the reported pore size to 25 nm. The 8.25-fold surface-area increase indicates that the clay phase and oven-dried composite structure created substantially more nitrogen-accessible surface than the compact cellulose alone. A pore size of approximately 25 nm lies in the mesoporous range and can facilitate transport of hydrated ions through the packed material. Increased surface area does not guarantee proportional fluoride uptake, but it generally improves the probability that reactive mineral and hydroxyl sites are contacted during flow.

The values are modest compared with highly activated carbons or some engineered metal-organic sorbents, yet they may be sufficient when combined with ion-exchange and surface-complexation sites. Montmorillonite contributes basal surfaces and edge hydroxyls, while cellulose maintains dispersion and forms a physically manageable matrix. The observed structural improvement is consistent with the wider literature on nanocellulose-based water-treatment media, where the polymer network serves as a scaffold for higher-affinity inorganic phases (Das *et al*., 2022). It is also consistent with reports that montmorillonite composites can improve contaminant access, reduce aggregation, and enhance hydraulic stability (Zango *et al*., 2022).

Taken together, the SEM, EDX, XRD, FTIR and BET observations are consistent with incorporation of a mineral phase into a cellulose-containing material. They do not distinguish covalent cross-linking from physical association. Identically processed cellulose-only and purified-clay controls were not available for comparison, so the contributions of clay addition, citric acid, heating and grinding to the surface-area change cannot be separated.

Effect of Operating Conditions in the Fixed-Bed Column

Each operating variable was varied one at a time while the others were held at fixed values that differed between series (Section 2.6), so the four series are not directly comparable and their best values should not be read as a combined optimum. Removal responded differently to each variable (Figure 4 and Table 2). Packed adsorbent mass was tested from 3 to 12 g, with the highest fluoride removal of 79.83% at 10 g (Figure 4A). A larger packed mass would normally be expected to provide more available sites and a longer mass-transfer zone, but removal at 12 g was lower than at 10 g, which may reflect channeling, differences in packing or experimental variability rather than a simple mass effect. In practical design, any gain from more media must be balanced against pressure drop, media cost and the volume of spent adsorbent generated.

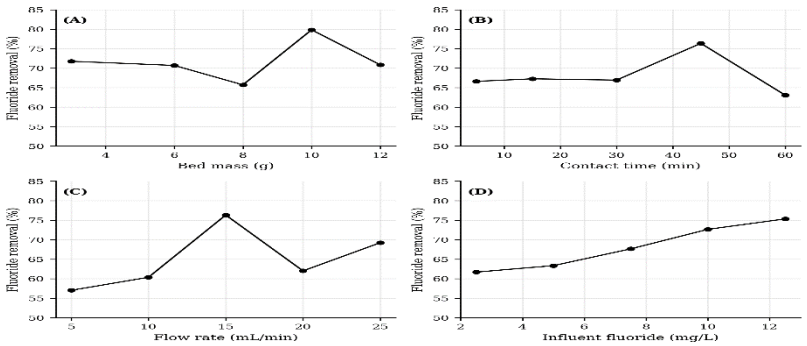


Figure 4: Reported effects of (A) packed adsorbent mass, (B) operating time, (C) influent flow rate, and (D) influent fluoride concentration on fluoride removal in the fixed-bed column. Points are the summarized values

Removal was similar (about 67%) at 5 to 30 min, peaked at 76.36% at 45 min and fell at 60 min (Figure 4B). An initially conditioned, constant-feed column would generally show increasing breakthrough as capacity is consumed. The peak in removal at 45 min is not explained by the available summary. They may reflect experimental variability, partial desorption, changing influent or effluent conditions, or the onset of bed saturation. Because replicate error bars were not available, the magnitude and statistical significance of these differences cannot be determined.

The flow-rate series showed the highest reported removal of 76.33% at 15 mL/min. At very high flow, residence time is shortened and intraparticle diffusion becomes less complete, which usually reduces removal. The lower values at 5 and 10 mL/min, followed by improvement at 15 mL/min, suggest that hydraulic distribution and channeling may also have influenced the column. Moderate flow can sometimes improve external mass transfer while retaining sufficient residence time. Similar interactions between residence time and film transfer have been observed in fixed-bed fluoride systems using alumina and polymer-supported sorbents (Kumari *et al*., 2021; Mani & Bhandari, 2022). Removal then fell at 20 mL/min and rose again at 25 mL/min, so the flow-rate response was not monotonic and cannot be attributed to residence time alone without replicate runs.

Increasing influent fluoride concentration from 2.5 to 12.5 mg/L raised the reported percentage removal to 75.34%. A higher concentration increases the driving force for mass transfer and can improve utilization of available sites before saturation. In many fixed-bed systems, however, high concefntration also causes earlier breakthrough because the finite capacity is consumed more rapidly. The positive percentage-removal trend in this experiment should therefore be interpreted together with breakthrough time and treated volume, not as evidence that service life necessarily improves at higher influent concentration.

Table 2: Summary of Fixed-Bed Operating-Variable Results

Variable	Tested range	Condition with highest removal	Removal at that condition (%)	Process interpretation
Packed adsorbent mass	3–12 g	10 g	79.83	Highest removal at 10 g; response not monotonic across 3–12 g.
Contact time	5–60 min	45 min	76.36	Peak at 45 min; lower at 60 min.
Flow rate	5–25 mL/min	15 mL/min	76.33	Peak at 15 mL/min; response not monotonic.
Influent fluoride	2.5–12.5 mg/L	12.5 mg/L	75.34	Removal rose with influent concentration; breakthrough time not reported.

Note. The adsorbent-mass series is expressed as packed adsorbent mass (g), not bed height (cm). Each series varied one factor with the other conditions held at values that differed between series, so the best conditions are not a combined optimum.

Residual fluoride was calculated from Equation (1) where both the influent concentration and removal were stated. At C_0 = 12.5 mg/L, removal of 76.36% in the operating-time series, 76.33% in the flow-rate series and 75.34% at the highest influent-concentration condition corresponds to C_t = 2.955, 2.959 and 3.083 mg/L, respectively. Removal of 55.42% in the fifth reuse cycle corresponds to 5.573 mg/L. These are calculated concentrations, not additional measurements. Each exceeds the 1.5 mg/L guideline cited here (WHO, 2022). A 12.5 mg/L feed requires at least 88% removal to reach 1.5 mg/L. Missing influent concentrations prevent the same assessment for the mass series and borehole waters.

Reuse Performance

The regenerated composite retained measurable activity over five cycles, but removal decreased from 76.36% in the first cycle to 71.51%, 68.75%, 58.69%, and 55.42% in cycles two through five, respectively (Figure 5A). Relative to the first cycle, the fifth-cycle value represents retention of approximately 72.6% of the initial removal performance. The decline may arise from incomplete desorption of fluoride, irreversible occupation of high-affinity sites, loss of fine particles during washing, pore blockage, or structural changes caused by repeated wetting and regeneration.

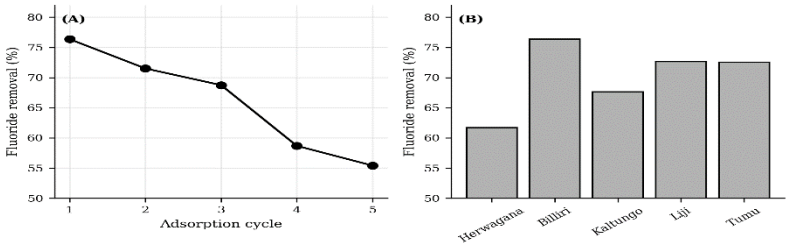


Figure 5: (A) Fluoride removal across five adsorption-regeneration cycles and (B) fluoride removal from borehole water collected in five communities in Gombe State

For a field-deployable adsorbent, regeneration must be assessed not only by percentage removal but also by recovered capacity, chemical demand, media mass loss, mineral leaching, effluent toxicity, and management of fluoride-rich regenerant. The observed five-cycle retention is promising for a simple biopolymer-clay material, but optimization of regeneration conditions is needed. Immobilized montmorillonite-containing cellulose materials have shown that a stable biopolymer framework can improve separation and reuse of fine mineral phases (Nehra *et al*., 2022). The present material would benefit from testing different regenerants and from mechanical-strength measurements before and after cycling.

Fluoride concentrations in the regenerant, media mass loss and post-cycle characterization were not available. The decline in performance therefore cannot be assigned to a

specific cause. Incomplete desorption, fines loss, pore blockage and structural change remain hypotheses requiring eluate analysis, fluoride mass balances and characterization before and after regeneration.

Borehole-Water Treatment and Matrix Effects

The composite removed fluoride from all five borehole waters, with reported efficiencies of 61.69% for Herwagana, 76.36% for Billiri, 67.65% for Kaltungo, 72.66% for Liji, and 72.55% for Tumu (Figure 5B and Table 3). The range confirms that the material remained active in natural waters containing dissolved salts and suspended matter. The lower removal for Herwagana may reflect differences in initial fluoride concentration, alkalinity, hardness, chloride, dissolved organic matter, or other competing species that were not fully quantified. Natural-water testing is important because laboratory solutions generally overestimate adsorption when competing anions and mineral colloids are absent.

Table 3: Physicochemical Properties and Reported Fluoride Removal for Borehole-Water Samples

Sample	pH	Conductivity	TDS	Turbidity	DO	Hardness	Chloride	F removal (%)
Distilled water	6.6	0.8	0.9	0.4	6.1	0	0.3	Not tested
Herwagana	7.3	221	119	5	8.0	122	32	61.69
Billiri	7.7	339	164	10	7.5	165	35	76.36
Kaltungo	6.9	287	175	13	7.2	212	44	67.65
Liji	7.4	344	138	6	6.8	145	52	72.66
Tumu	7.6	392	220	15	6.0	190	60	72.55

Sample pH values ranged from 6.9 to 7.7, a near-neutral interval relevant to drinking-water treatment. Conductivity and TDS were highest in Tumu, while Kaltungo had the greatest reported hardness. Chloride ranged from 32 to 60 in Table 3. The fact that Billiri showed the highest removal despite moderate-to-high conductivity indicates that total ionic strength alone did not determine performance. Specific competing anions, especially bicarbonate, phosphate, sulfate, and silicate, are often more informative for fluoride adsorption than bulk conductivity. Future work should quantify these ions and use controlled competition experiments to clarify selectivity.

A practical endpoint is the treated fluoride concentration rather than percentage removal alone. If an influent concentration is far above the WHO guideline, removal of approximately 60-80% may still leave an effluent above 1.5 mg/L. The material should therefore be evaluated using breakthrough criteria based on a health-protective effluent limit, with treated volume per unit mass reported at breakthrough and exhaustion. Such reporting would permit direct comparison with natural clay, modified alumina, and engineered composite columns (Wan *et al*., 2021; Kumari *et al*., 2021).

Column-Model Performance

The reported Thomas linear regression had a slope of −0.0857 min^{-1} and an intercept of 3.36. The Yoon–Nelson coefficients were 0.0857 min^{-1} and −3.36, giving $\tau = 3.36/0.0857 = 39.21$ min. These coefficient pairs describe the same logistic curve, rather than independent evidence of model agreement. The reported R^2 values of approximately 0.96 and 0.98 are inconsistent for identical observations fitted by these linear transformations and remain unverified (Table 4).

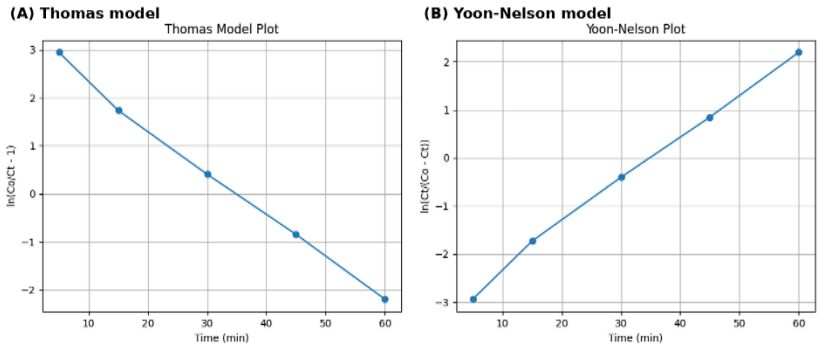


Figure 6: Illustrative linearized Thomas and Yoon–Nelson plots reconstructed from the reported regression coefficients. The graphics are not experimental breakthrough observations and cannot validate goodness of fit. Any displayed R^2 labels are unverified summary values

Table 4: Reported Fixed-Bed Model Parameters

Model	Slope (min^{-1})	Intercept	Rate constant	Capacity or time	Reported R^2	Status
Thomas	−0.0857	3.36	Unverified	244.9 mg/g unverified	0.96	Refit required
Yoon–Nelson	0.0857	−3.36	0.0857 min^{-1}	τ = 39.21 min	0.98	Refit required

Note. Regression coefficients are reproduced from the supplied summary and have not been independently refitted. The reported capacity of 244.9 mg/g is not accepted as a validated result. Model-specific operating conditions and raw observations are required to resolve capacity and R^2 inconsistencies.

A feed mass balance provides an essential capacity check. For a 10 g bed operated at C_0 = 12.5 mg/L and Q = 0.005 L/min for 45 min, the total fluoride supplied is 2.8125 mg; uptake over that interval cannot exceed 0.28125 mg/g. Thus, 244.9 mg/g cannot represent uptake over that interval under those conditions. If, and only if, these were also the model-fitting conditions, the coefficients would give kTh = 0.0857/12.5 = 0.006856 L mg^{-1} min^{-1} and $q_0 = 3.36 \times 0.005/(0.006856 \times 10)$ = 0.2450 mg/g. This conditional calculation suggests a possible factor-of-1000 unit conversion error, but does not establish a corrected experimental capacity. In addition, τ = 39.21 min implies 50% removal at that time, whereas 76.36% removal was reported at 45 min. The two summaries cannot represent the same ideal breakthrough curve under identical conditions without further explanation.

Measured C_t/C_0 observations, the complete run duration and the model-specific C_0, Q and m are required before refitting. Experimental breakthrough curves, prediction residuals, SSE, RMSE and parameter confidence intervals cannot be recovered reliably from slopes and intercepts alone. No synthetic observations or invented error statistics have been substituted for those records.

Proposed Adsorption Mechanisms

The characterization and performance trends support a multimechanistic interpretation. First, hydrated fluoride can interact with protonated edge hydroxyl groups on montmorillonite through electrostatic attraction and ligand exchange. Second, exchangeable interlayer or surface-associated cations may contribute to ion exchange or formation of metal-fluoride surface complexes. Third, the hydroxyl-rich cellulose network can retain water, disperse the clay, and provide hydrogen-bonding environments that improve contact between the solution and mineral domains. Fourth, the enlarged mesoporous structure can reduce transport limitations by providing pathways to internal sites.

The near-neutral pH of the natural waters suggests that adsorption did not require strongly acidic conditions, which is beneficial for drinking-water application. Still, fluoride affinity usually decreases as pH rises and hydroxide competes for mineral sites. The present study did not report a controlled pH series or point of zero charge. A mechanistic follow-up should therefore measure zeta potential, pH at the point of zero charge, fluoride uptake over a broad pH range, and release of Al, Si, Fe, and other elements. Spectroscopy of the material before and after fluoride adsorption would help distinguish physical retention from ligand exchange and mineral precipitation.

Study Limitations and Implications for Scale-Up

The available results support a preliminary descriptive assessment. Replicate-level records, uncertainty estimates and complete analytical quality-control information were not available for review. Experimental replication and recovery of the original records are required before claims of reproducibility or statistical significance can be assessed.

For stronger method reproducibility, the fluoride analytical protocol should report the reagent formulation, analytical wavelength, calibration range, detection limit, quality-control recovery, blanks, duplicates and sample replication. The real-water table should also retain consistent unit metadata for every physicochemical parameter.

The term composite is used in preference to nanocomposite because direct particle-size evidence was not obtained. The nanoscale coherent crystallite dimensions from Scherrer analysis describe diffracting domains, not particle size. Transmission electron microscopy, dynamic light scattering for dispersible fractions, or atomic-force microscopy would be needed to support any nanoscale classification. XRD interpretation should also include raw clay, extracted cellulose, and composite patterns measured under identical conditions, with the montmorillonite basal reflection and d-spacing explicitly reported.

Column evaluation should be expanded to full breakthrough curves at several bed depths, influent concentrations, and flow rates. Treated bed volumes, empty-bed contact time, breakthrough capacity, exhaustion capacity, mass-transfer-zone length, pressure drop, and hydraulic conductivity should be reported. The Bed Depth Service Time model could then support scale-up. Long-duration runs are required to determine whether cellulose swelling, microbial growth, clay-fine release, or channeling alters performance.

Material safety is central to drinking-water use. The composite should be tested for leaching of aluminium, iron, manganese, zinc, copper, and other EDX-detected elements. Acute and chronic toxicity screening of treated water, together with total organic carbon and turbidity measurements, would identify unwanted releases. Regeneration studies should quantify fluoride in the desorption solution, media mass loss, and adsorption capacity rather than removal percentage alone. A life-cycle and cost analysis should compare banana-stem collection, chemical consumption, oven-drying energy, column replacement, and regenerant disposal with established adsorbents.

Conclusion

The study demonstrated the potential of a banana pseudostem cellulose–montmorillonite composite for fluoride removal from water under laboratory fixed-bed adsorption conditions. Composite preparation increased the reported specific surface area, while the adsorption experiments showed that fluoride removal was influenced by operational conditions. The highest reported removal efficiency was 79.83%, and the composite exhibited measurable adsorption performance when applied to selected borehole-water samples. However, declining efficiency during repeated use indicates limitations in regeneration and long-term operational stability. Further studies should investigate adsorption mechanisms, breakthrough behavior, competing-ion effects, material leaching, uncertainty and the final fluoride concentrations in treated water. These investigations are necessary to establish the technical reliability and practical suitability of the composite for groundwater defluoridation.

REFERENCES

American Public Health Association, American Water Works Association, & Water Environment Federation. (2023). *Standard methods for the examination of water and wastewater* (24th ed.). APHA Press.

Das, R., Lindström, T., Sharma, P. R., Chi, K., & Hsiao, B. S. (2022). Nanocellulose for sustainable water purification. *Chemical Reviews*, *122*(9), 8936–9031. https://doi.org/10.1021/acs.chemrev.1c00683

Kalsido, A. W., Meshesha, B. T., Behailu, B. M., & Alemayehu, E. (2021). Optimization of fluoride adsorption on acid modified bentonite clay using fixed-bed column by response surface method. *Molecules*, *26*(23), Article 7112. https://doi.org/10.3390/molecules26237112

Kumari, U., Mishra, A., Siddiqi, H., & Meikap, B. C. (2021). Effective defluoridation of industrial wastewater by using acid modified alumina in fixed-bed adsorption column:

Experimental and breakthrough curves analysis. *Journal of Cleaner Production*, *279*, Article 123645. https://doi.org/10.1016/j.jclepro.2020.123645

Mani, S. K., & Bhandari, R. (2022). Efficient fluoride removal by a fixed-bed column of self-assembled Zr(IV)-, Fe(III)-, Cu(II)-complexed polyvinyl alcohol hydrogel beads. *ACS Omega*, *7*(17), 15048–15063. https://doi.org/10.1021/acsomega.2c00834

Merais, M. S., Khairuddin, N., Salehudin, M. H., Siddique, M. B. M., Lepun, P., & Chuong, W. S. (2022). Preparation and characterization of cellulose nanofibers from banana pseudostem by acid hydrolysis: Physico-chemical and thermal properties. *Membranes*, *12*(5), Article 451. https://doi.org/10.3390/membranes12050451

Nagaraj, A., Pillay, K., Kumar, S. K., & Rajan, M. (2020). Dicarboxylic acid cross-linked metal ion decorated bentonite clay and chitosan for fluoride removal studies. *RSC Advances*, *10*, 16791–16803. https://doi.org/10.1039/D0RA00598C

Nascimento, R. E. A., Carvalheira, M., Crespo, J. G., & Neves, L. A. (2023). Extraction and characterization of cellulose obtained from banana plant pseudostem. *Clean Technologies*, *5*(3), 1028–1043. https://doi.org/10.3390/cleantechnol5030052

Nehra, S., Dhillon, A., Sharma, R., Nair, M., & Kumar, D. (2022). Water-dispersible magnetite montmorillonite encapsulated cellulose beads for fluoride removal and their kinetics and mechanism. *Environmental Nanotechnology, Monitoring & Management*, *18*, Article 100690. https://doi.org/10.1016/j.enmm.2022.100690

Nwabanne, J. T., & Igbokwe, P. K. (2012). Adsorption performance of packed bed column for the removal of lead (II) using oil palm fibre. *International Journal of Applied Science and Technology*, *2*(5), 106–115.

Solanki, Y. S., Agarwal, M., Gupta, A. B., Gupta, S., & Shukla, P. (2022). Fluoride occurrences, health problems, detection, and remediation methods for drinking water: A comprehensive review. *Science of the Total Environment*, *807*, Article 150601. https://doi.org/10.1016/j.scitotenv.2021.150601

Wan, K., Huang, L., Yan, J., Ma, B., Huang, X., Luo, Z., Zhang, H., & Xiao, T. (2021). Removal of fluoride from industrial wastewater by using different adsorbents: A review. *Science of the Total Environment*, *773*, Article 145535. https://doi.org/10.1016/j.scitotenv.2021.145535

World Health Organization. (2022). *Guidelines for drinking-water quality: Fourth edition incorporating the first and second addenda*. World Health Organization.

Yahya, M. D., Aliyu, A. S., Obayomi, K. S., Olugbenga, A. G., & Abdullahi, U. B. (2020). Column adsorption study for the removal of chromium and manganese ions from electroplating wastewater using cashew nutshell adsorbent. *Cogent Engineering*, *7*(1), Article 1748470. https://doi.org/10.1080/23311916.2020.1748470

Yohanna, A., Musa, N., Balogun, F. O., Agada, E. A., Adamu, A., & Galumje, S. S. (2022). Investigation of groundwater contamination in some selected areas of Bogoro and environs, North-East Nigeria. *FUDMA Journal of Sciences*, *6*(1), 358–367. https://doi.org/10.33003/fjs-2022-0601-907

Zango, Z. U., Garba, A., Garba, Z. N., Zango, M. U., Usman, F., & Lim, J.-W. (2022). Montmorillonite for adsorption and catalytic elimination of pollutants from wastewater: A state-of-the-arts review. *Sustainability*, *14*(24), Article 16441. https://doi.org/10.3390/su142416441

Zhang, M. (2024). Enhanced fluoride removal using montmorillonite clay modified with CoFe2O4 and metal-organic frameworks. *Environmental Research*, *258*, Article 119389. https://doi.org/10.1016/j.envres.2024.119389

©2026 This is an Open Access article distributed under the terms of the Creative Commons Attribution 4.0 International license viewed via https://creativecommons.org/licenses/by/4.0/ which permits unrestricted use, distribution, and reproduction in any medium, provided the original work is cited appropriately.